SOUNDINGS OF TERRESTRIAL RADIATION FLUX OVER WISCONSIN[1]

P. M. KUHN, Office of Meteorological Research, U.S. Weather Bureau

V. E. SUOMI and G. L. DARKOW, Department of Meteorology, The University of Wisconsin

[Manuscript received January 6, 1959; revised April 7, 1959]

ABSTRACT

Results and conclusions drawn from 50 radiometer-sonde ascents over Wisconsin are presented. Atmospheric infrared radiation flux is separated into upward, downward, and net components. Radiation divergence and resulting cooling are computed. Seasonal averages of these direct observations are compared.

1. INTRODUCTION

In the past, direct measurements of the atmosphere's radiative balance have been costly and complex. Suomi, Staley, and Kuhn [1] recently reported on a radiometer-sonde which was designed as a routine technique for obtaining vertical profiles of the flux of infrared radiation in the atmosphere. This instrument has been successfully adapted to balloon-borne flights, and briefly, consists of the economical net radiometer described by Suomi and Kuhn [2] attached to the standard U.S. Weather Bureau radiosonde. An electrically driven sequencer and simple circuit modifications are necessary.

SYMBOLS USED IN TEXT

$\partial T/\partial t$	Change in temperature in °C. per day.
g	Acceleration due to gravity, c.g.s. units.
R_{NU}	Net radiation in langleys per minute at top of layer ($R_{NU}>0$ directed upward).
R_{NL}	Net radiation in langleys per minute at bottom of layer ($R_{NL}>0$ directed upward).
c_p	Specific heat of air, c.g.s. units.
Δp	Thickness of layer in millibars.
σ	Stefan-Boltzmann constant, c.g.s. units.
T_b	Observed temperature of bottom sensor.
T_t	Observed temperature of top sensor.
C_i	Internal conduction for radiometer in langleys per minute.
C_t	Top conduction for radiometer in langleys per minute.
C_b	Bottom conduction for radiometer in langleys per minute.
E_b	Error term for bottom half of radiometer, langleys per minute.
E_t	Error term for top half of radiometer, langleys per minute.

NOTE.—Values of radiation flux or net radiation >0 indicate a flux or net flux directed away from the air-ground interface.

[1]The research reported in this study is supported by the Office of Meteorological Research, U.S. Weather Bureau.

2. TYPICAL RADIOMETER FLIGHTS

The radiometer-sonde flights were carried out at the University of Wisconsin at Madison, Wis. The flight program included (i) direct measurement of the upward, downward, net, and total components of infrared radiation flux; and (ii) computation of radiative cooling of the atmosphere.

Figures 1 through 3 show three typical nocturnal ascents. In each, the upward, $R\uparrow$, downward, $R\downarrow$, and net, R_N, radiation currents in langleys per minute are shown, together with the air and dewpoint temperatures. The radiative temperature change of the air column is calculated from the vertical divergence of radiation in 50-mb. layers up to the 200-mb. level and for 25-mb. layers above that from the expression,

$$\frac{\partial T}{\partial t}=\frac{-g(R_{NU}-R_{NL})}{c_p\Delta p} \tag{1}$$

This profile, given in degrees Celsius change per day, appears on the right for each figure.

Figure 1 is a clear summer night sounding and illustrates characteristic features of many similar flights. In all such cases relative warming occurs just beneath any inversion, including the tropopause. In particular, the warming was evident at 815 mb. during the flight of July 7, 1958, beneath a low-level inversion. Again at 270 mb., warming occurred beneath the tropopause inversion. The latter phenomenon is clearly visible immediately below the tropopause in the summer mean cooling profile. Frequently, such radiative warming becomes positive, at times reaching from 2° to 3° Celsius heating per day. For example, a warming of 1.0° C. per day occurred at 270 mb. on the July 7, 1958, ascent.

Secondly, in many instances we find the strongest cooling just above inversions or cloud layers. In detail, this may be seen in figure 1 at 680 and 165 mb., reaching over 2.0° C. in each case. Figure 1 might be compared with the observed cooling rate obtained by Brewer and Houghton [3] for July 20 and 21, 1956.

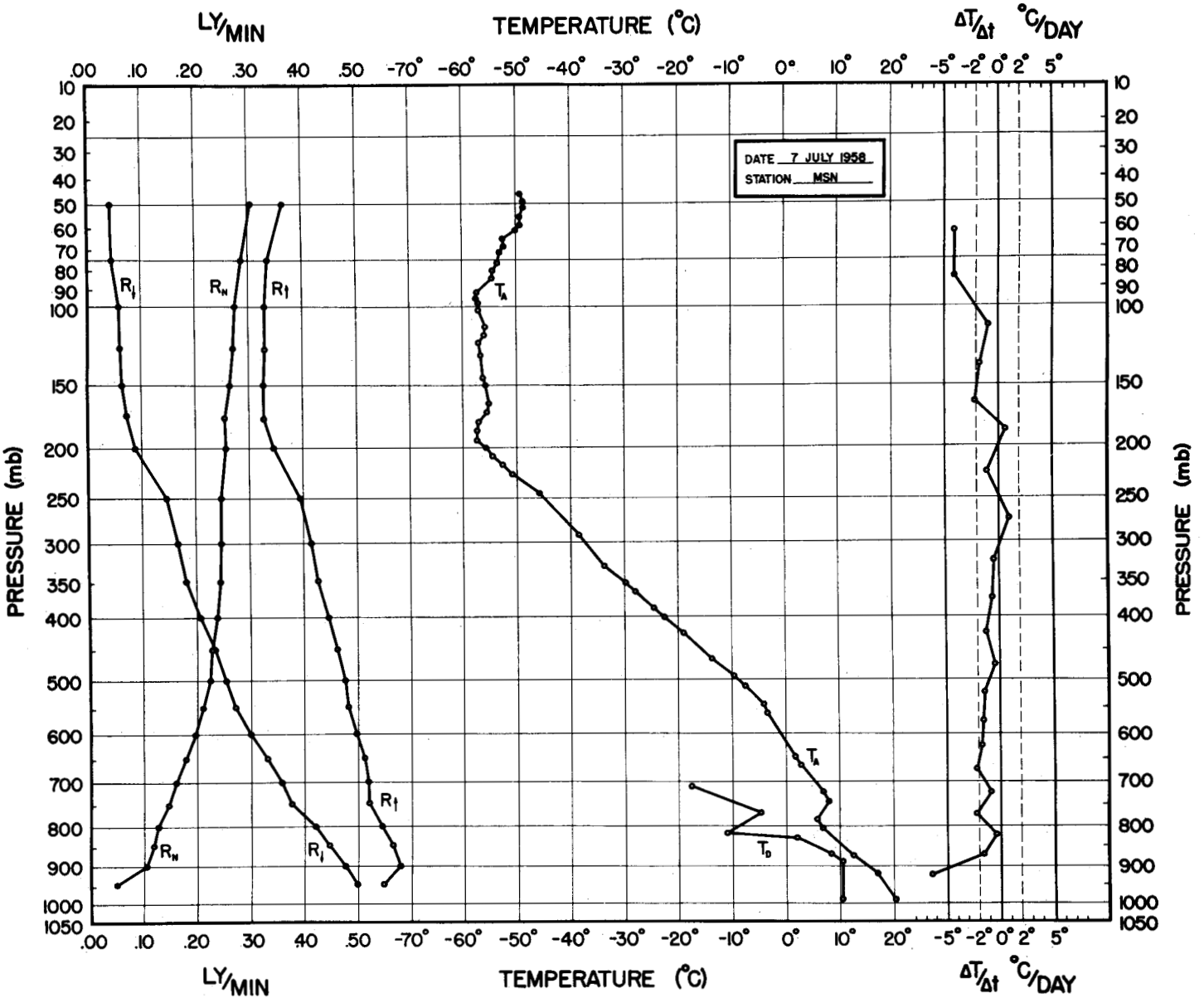

FIGURE 1.—Clear summer radiometer-sonde ascent. July 7, 1958, 2000 CST, Madison, Wis.

The clear nocturnal winter sounding, figure 2, provides a typical cooling profile often observed in the winter. The average cooling of this winter profile, except for the microlayer, is 1.0° C. per day, as compared with a summer average cooling rate of 1.7° C. per day. Thus direct radiation measurements allow a computation of radiative cooling far above the limits of chart evaluation. Between 250 and 200 mb., there is indication of the ascent passing above effective atmospheric radiators. Both the upward and downward radiation currents approach a constant value even though there is a positive gradient in the temperature profile. The last plotted point in the upward stream is doubtful.

A cloudy winter ascent, figure 3, demonstrates the radiative effects of cloud. Below the stratocumulus base at 870 mb. there is radiative warming. At the cloud top, however, there is a sharp gradient in the downward directed radiation, $R\downarrow$, resulting in strong radiative divergence and a cooling rate of 8.5° C. per day. The break into the clear night sky at 725 mb. sharply reduces the downward propagating current. The gradient of $R\downarrow$ increases from −0.03 ly./min. per 50 mb. to −0.09 ly./min. per 50 mb. In the layer between 100 and 150 mb., regardless of slowly falling air temperatures, the upward and downward radiation currents become essentially constant. This further indicates a decrease in atmospheric radiators.

3. AVERAGE SOUNDINGS

CLEAR WINTER

An average cooling rate for clear winter ascents was obtained by averaging the upward, downward, and net components of the radiative flux in 50-mb. steps for 12

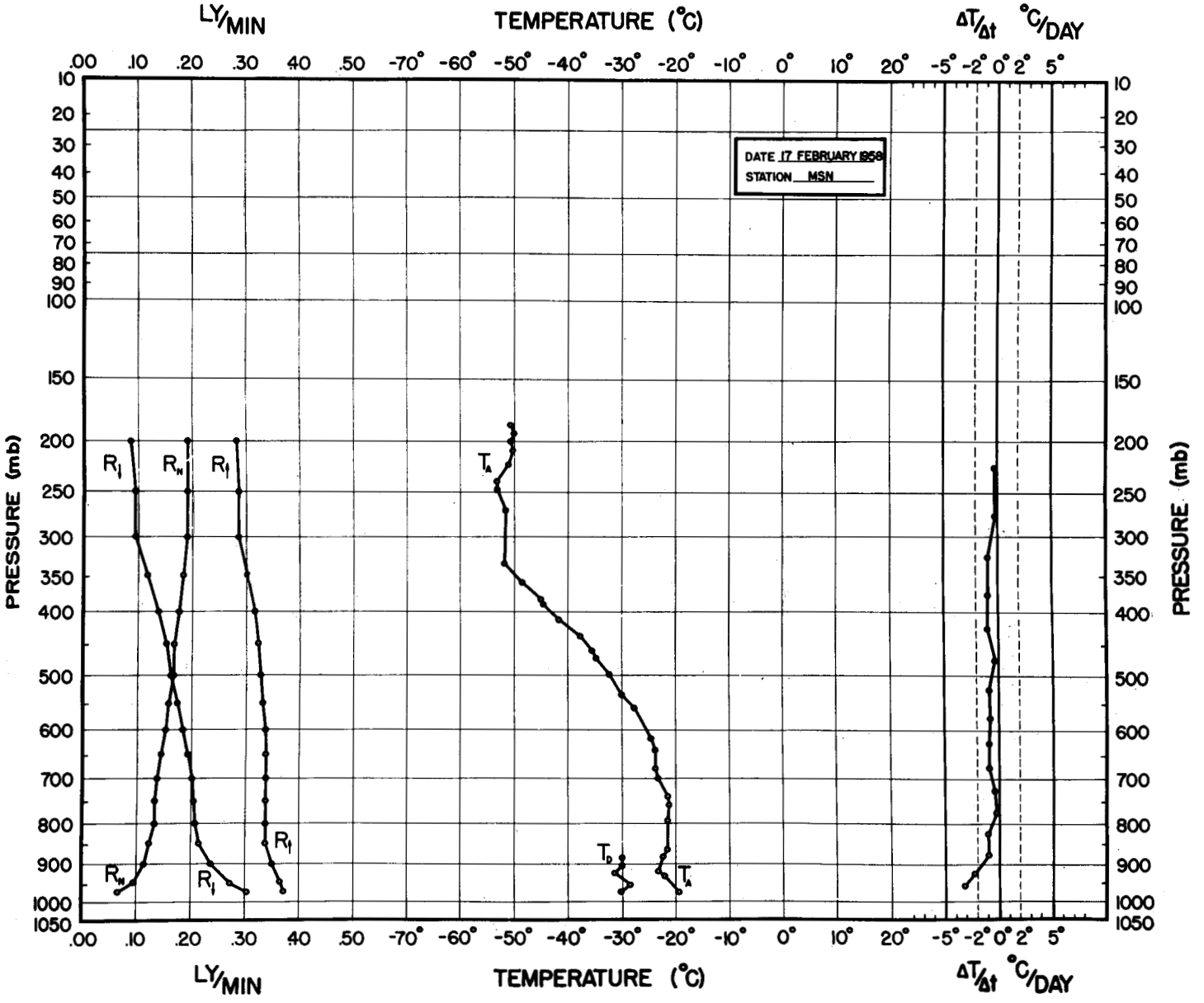

FIGURE 2.—Clear winter radiometer-sonde ascent. February 17, 1958, 2136 CST, Madison, Wis.

ascents. Cooling was then computed from these results providing a mean vertical distribution of the terrestrial radiation and its divergence. A simple computation, equation (1), gives the profile of cooling. In figure 4 this average cooling is compared with Möller's [4] indirect estimate of the mean mid-latitude annual infrared cooling. Except for the observed decrease in cooling just beneath the mean height of the tropopause, the indirect estimates coincide favorably with the directly measured cooling. London's [5] computation of the mean March infrared cooling also lies well within a comparable range but is offset in season. Between 150 and 200 mb. there is a tendency for constancy in $R\downarrow$ and $R\uparrow$, though it is not as evident as in the average summer profiles.

CLEAR SUMMER

The 12 summer flights, reaching a mean height of 75 mb., furnish a representative mid-latitude average of the vertical distribution of radiative fluxes and the infrared atmospheric cooling for a continental climate. The data of figure 5 are presented in the manner of figure 4.

Between 70 and 150 mb. in the average summer soundings, the gradient of the downward- and upward-directed radiation fluxes tends to zero. This indicates that under clear summer conditions there exists a marked decrease in atmospheric radiators near the 100-mb. level and above. The mean cooling averages 1.7° C. per day compared with a mean winter cooling of 1.0° C. per day.

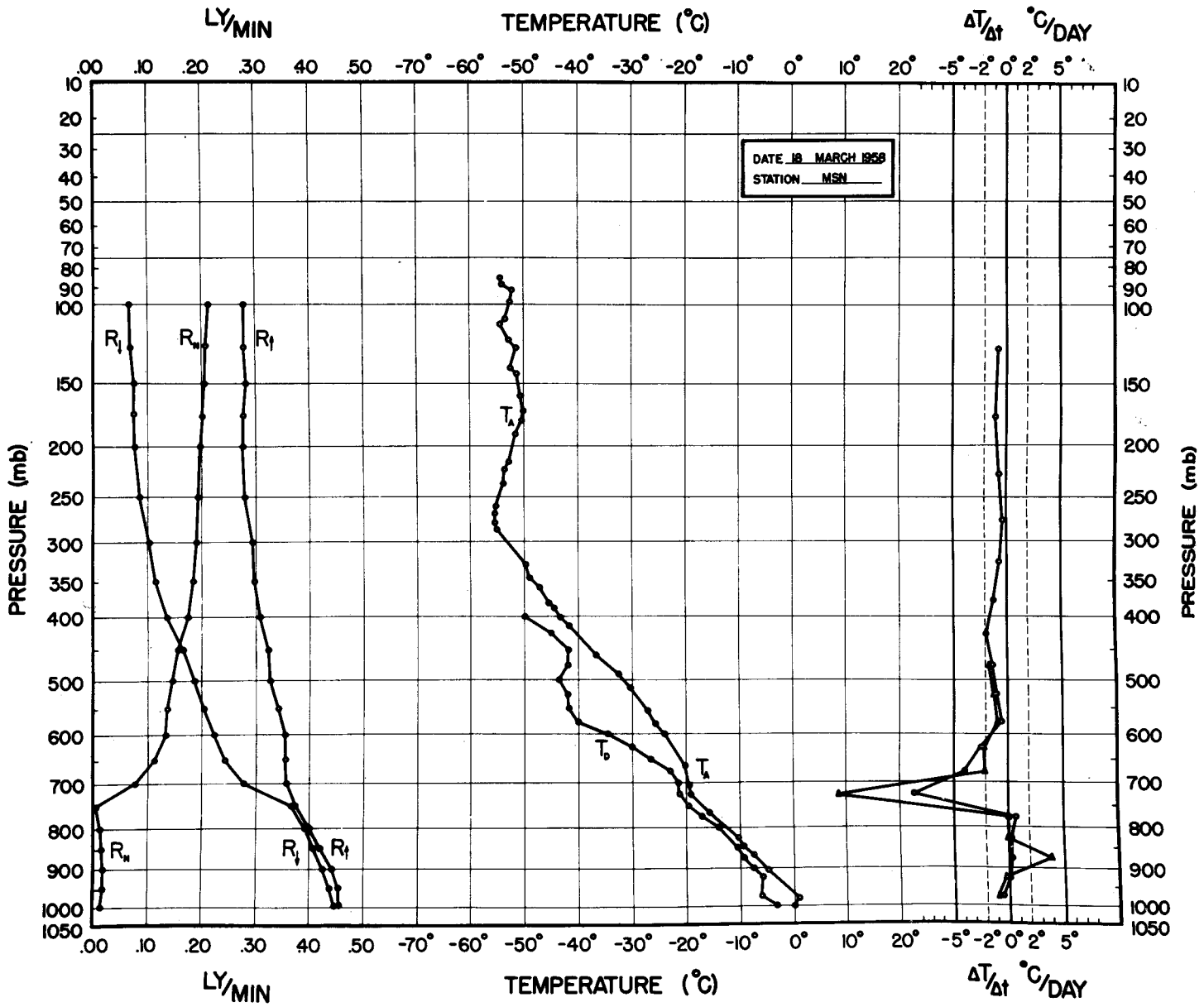

FIGURE 3.—Cloudy winter radiometer-sonde ascent. March 18, 1958, 2033 CST, Madison, Wis. Triangles represent Elsasser cooling evaluation. Circles indicate direct evaluation of radiative cooling.

4. TERRESTRIAL RADIATION

The values of this outgoing terrestrial (net) radiation for only the highest flights, clear and cloudy, in which the observed vertical gradient of the net radiation becomes zero, are averaged in table 1. For comparison, the estimates of Robinson [6] at Kew, Lettau [7] for Northern Hemisphere annual average, and Houghton [8] for Northern Hemisphere annual average are included.

TABLE 1.—*Outgoing terrestrial (net) radiation, langleys per minute*

Summer		Annual		Winter	
Madison Average	0.310	Lettau	0.320	Madison Average	0.220
Robinson (Kew)	.320	Houghton	.320	Robinson (Kew)	.270
		Madison	.265		

5. CLOUD EFFECTS

A characteristic phenomenon associated with ascents through clouds appears in figure 3 at 725 mb. Very strong radiative divergence immediately above a cloud top appears as an excellent indicator of the cloud top. This feature is obviously caused by the rapid decrease in the downward current of radiation measured by the upward-facing surface of the radiometer as it breaks into the clear night sky above the clouds.

6. ELSASSER CHART COMPARISON

The cooling profile indicated by triangular points in figure 3 represents an Elsasser evaluation for this flight

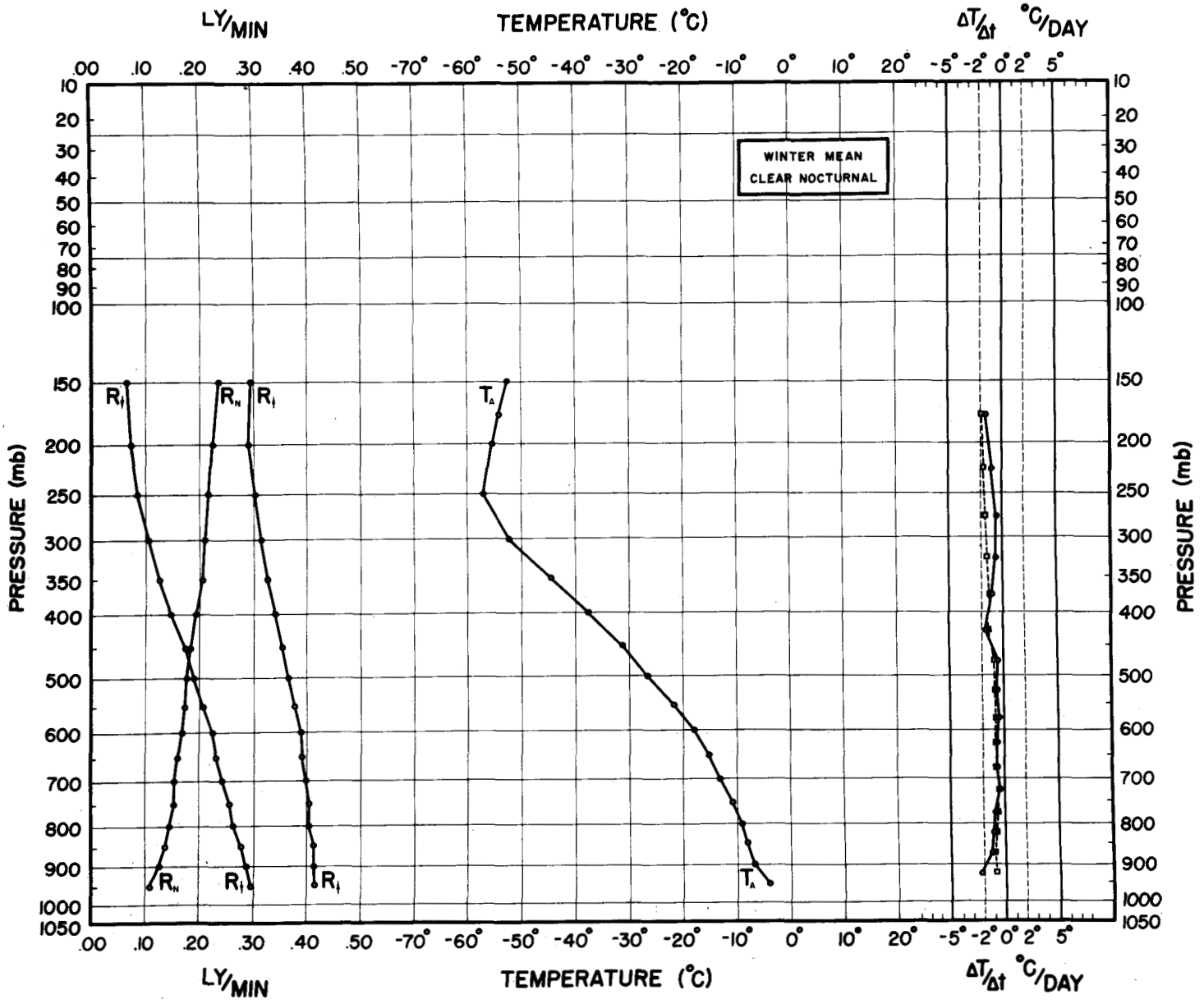

FIGURE 4.—Winter mean clear nocturnal ascent. Squares indicate annual cooling rate estimate by Möller.

Omitting that portion of the Elsasser [9] computation which is dependent upon assumptions made for the cloud emissivity, we find the general agreement between the direct and indirect cooling evaluation good. However, the humidity element was out of range above 450 mb., eliminating an Elsasser evaluation for nearly two-thirds of the ascent. On the basis of the indirect chart radiation evaluations for a limited number of flights, the radiation values appear somewhat underestimated when compared with our direct measurements. This will be the subject of a forthcoming report. The magnitude of the directly measured warming and cooling below and above cloud bases and tops agrees with indirect estimates of Möller [4].

7. PRACTICAL APPLICATIONS

Some of the apparent practical applications of the radiometer-sonde ascents are for cloud top determinations and in studies of cloud dissipation, propagation to the surface of high-level heating and cooling, stability changes, and the role of long-wave radiational destabilization as a trigger mechanism for nocturnal thunderstorms. The actual measurement of the infrared components under a variety of situations is providing a valuable tool with which these applications can be studied.

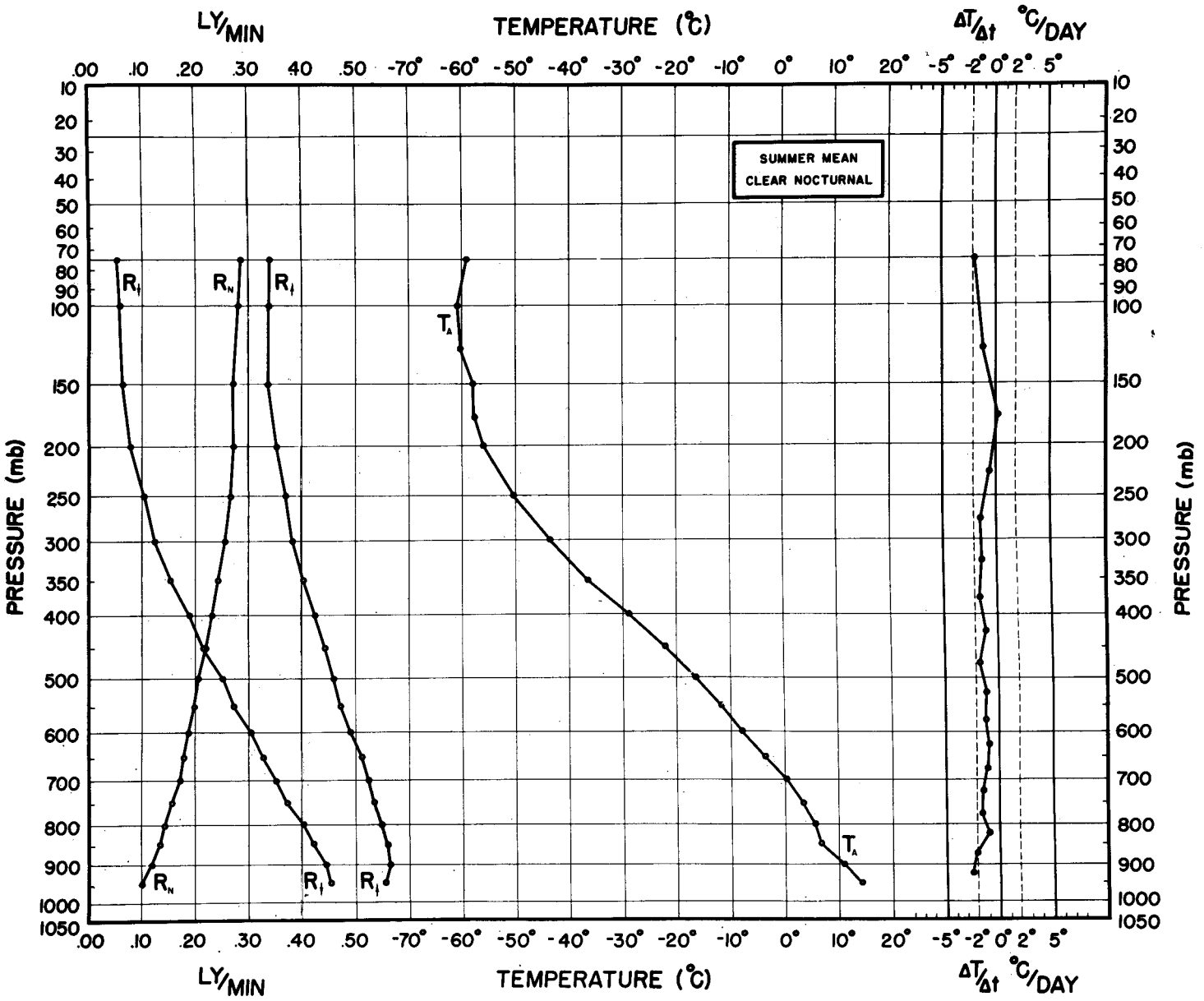

FIGURE 5.—Summer mean clear nocturnal ascent.

8. SATELLITE METEOROLOGY IMPLICATIONS

There is, of course, a natural tie between satellite radiation measurements and similar measurements with the radiometer-sonde. One might state that the balloon-borne radiometer fills in details integrated out by satellite measurements. Primarily, a radiometer-sonde network could augment the satellite measurements. Of necessity the satellite horizontally integrates radiation measurements of the earth and atmosphere over large areas because of its great speed and height. On the other hand, radiometer-sonde observations, though limited in height, provide exceptional vertical detail over a limited area. The satellite measures the large-scale radiation balance of the earth-atmosphere system from a point in space. The radiometer-sonde measures radiative fluxes within the earth-atmosphere system.

9. ACCURACY OF MEASUREMENTS

Standard calibration procedure includes a separate base line check at three temperatures of the three thermistors used in each flight, together with a surface check of the actual net radiation against a suitable standard.

Many additional tests and precautions, their actual details too extensive for this report, are either routinely performed in preparation for each flight or have been conducted as controlled experiments. Among these are the following:

1. Dry nitrogen purging of each radiometer prior to flight to prevent internal moisture condensation.

2. Individual calibration of the three thermistor sensors to prevent systematic errors.

3. Use of proportional changes in both vertical and

horizontal dimensions of the radiometer as a check on validity of the conduction terms.

4. Use of discrete changes in length of flight train as a check on solid angle intercept of balloon in affecting radiation measurement.

5. Substitution of bead thermistors for standard rod thermistors to improve lag characteristics of radiation sensing surfaces.

6. Extensive computations of transmissivity of polyethylene ventilation shield cells covering range from 0.8 to 40 microns.

7. Extending emissivity calculations for blackening agent, black "Decoret" Enamel, to 40 microns.

8. Comparison, in flight, of single- and double-layer polyethylene ventilation shields as to their respective effects on the ratio of conduction to convection transfers in these horizontal layers.

9. Tests of effects of nonhorizontal orientation of radiometer in flight by means of pendulum effect.

10. Evaluation of validity of internal conduction term, C_i, in equation (1) through its elimination in a comparison flight of a "disc" radiometer.

11. Determination of the profile of the gradient of temperature in the horizontal through the radiometer through multiple sensors.

The effects of a flight trajectory through clouds on the absolute accuracy of either $R\downarrow$ or $R\uparrow$ have not been completely determined. While it is believed that such effects on radiation measurements as moisture on the top polyethylene shield are rapidly eliminated due to ventilation, this is being carefully investigated. The rapid decrease in the magnitude of the downward propagating radiation current indicates a diminution in this assumed adverse effect immediately upon exit from cloud.

A careful error analysis has been made of the accuracy of temperature measurement including these random errors: thermistor error, thermistor lag, recorder error, calibration error, and transmitter error [10]. The "accuracy" ascribed to any measuring instrument may be misleading because of the many ways of estimating and expressing accuracy. Customarily, we employ various statistical measures of dispersion to indicate this accuracy and those most often used are the standard deviation, the average deviation, and the probable error. Their interrelation is well known. However, we will limit our error discussion to the standard deviation, σ. The root of the sum of squares of individually computed temperature measurement standard deviations in the error analysis mentioned above provides a value for one standard deviation, σ, of 0.4° C. Setting out confidence limits at 95 percent, we must accept a maximum error (2σ) of 0.8° C. Such a random error becomes most important in computing atmospheric cooling and can possibly result in maximum cooling errors of up to ±1.2° C. This maximum cooling rate error is large in comparison to some of the observed mean values, but it should be remembered that 95 percent of the errors will be less than 1.2° C. and 67 percent less than 0.6° C. We are experimenting with methods of reducing this maximum error to ±0.5° C. Such methods center primarily about a measurement of ΔT, the temperature difference between top and bottom sensors, rather than the absolute top and bottom temperatures, which can go far toward eliminating the inherent error in the small difference between two large numbers.

Consider the expression for net radiation, R_N,

$$R_N=\sigma(T_b^4-T_t^4) +1.37\left[2C_i+C_t-C_b+\lambda\frac{d}{dt}(T_b-T_t)+E_b-E_t\right] \quad (2)$$

Investigation reveals the relative size of the first and second terms on the right, the black-body and conduction terms, to be in the ratio 1.0 to 0.6 in the lower flight levels. At the tropopause this ratio changes to 1.0 to 1.8. Above the tropopause with the vertical change in the upward and downward radiation currents tending to zero, the lag term, third on right, becomes insignificant. The maximum size of the lag term never exceeds 5 percent of the net radiation and this occurs only in cases of extreme gradient of the observed top and bottom radiating temperatures.

REFERENCES

1. V. E. Suomi, D. O. Staley, and P. M. Kuhn, "A Direct Measurement of Infra-red Radiation Divergence to 160 mb.," *Quarterly Journal of the Royal Meteorological Society*, vol. 84, No. 360, Apr. 1958, pp. 134–141.
2. V. E. Suomi and P. M. Kuhn, "An Economical Net Radiometer," *Tellus*, vol. 10, No. 1, Feb. 1958, pp. 160–163.
3. A. W. Brewer and J. T. Houghton, "Some Measurements of the Flux of Infra-red Radiation in the Atmosphere," *Proceedings of the Royal Society (A)*, vol. 236, Aug. 1956, pp. 175–186.
4. F. Möller, "Long-Wave Radiation," *Compendium of Meteorology*, American Meteorological Society, Boston, Mass., 1951, pp. 34–49.
5. J. London, "The Distribution of Radiational Temperature Change in the Northern Hemisphere during March," *Geophysical Research Papers* No. 18, Geophysics Research Directorate, Air Force Cambridge Research Center, Bedford, Mass., 1952, 64 pp.
6. G. D. Robinson, "The Use of Surface Observations to Estimate the Local Energy Balance of the Atmosphere," *Proceedings of the Royal Society (A)*, vol. 236, Aug. 1956, pp. 160–171.
7. H. Lettau, "A Study of the Mass, Momentum, and Energy Budget of the Atmosphere," *Archiv für Meteorologie, Geophysik, und Bioklimatologie, Ser. A*, vol. 7, 1954, pp. 133–157.
8. H. G. Houghton, "On the Annual Heat Balance of the Northern Hemisphere," *Journal of Meteorology*, vol. 11, No. 1, Feb. 1954, pp. 1–9.
9. W. M. Elsasser, "Heat Transfer by Infrared Radiation in the Atmosphere," *Harvard Meteorological Studies*, No. 6, Harvard University, 1942, 107 pp.
10. Air Weather Service, "Accuracies of Radiosonde Data," *Air Weather Service Technical Report* 105–133, Washington, D.C., Sept. 1955.

508099—59——3